Functionalized Co_3O_4 Graphitic Nanoparticles: A High Performance Electrocatalyst for the Oxygen Evolution Reaction

N. Srinivasa,[1] L. Shreenivasa,[1] Prashanth S. Adarakatti[2,3], Robert D. Crapnell[3], Samuel J. Rowley-Neale[3,4], Ashoka Siddaramanna[1*] and Craig E Banks [3,4*]

[1]; Department of Chemistry, School of Engineering, Dayananda Sagar, University, Bengaluru, India

[2]; Department of Chemistry, SVM Arts, Science and Commerce College, Ilkal- 587125, India

[3]; Manchester Fuel Cell Innovation Centre, Manchester Metropolitan University, Chester Street, Manchester M1 5GD, UK

[4]; Faculty of Science and Engineering, Manchester Metropolitan University, Chester Street, Manchester M1 5GD, UK

*To whom correspondence should be addressed.

Email: ashok022@gmail.com and c.banks@mmu.ac.uk; Tel: ++(0)1612471196; Fax: ++(0)1612476831

1. Abstract

We describe a novel synthesis technique for the production of graphitic carbon functionalized Co_3O_4 (G/Co_3O_4), which involves the rapid decomposition of cobalt nitrate in presence of citric acid. Upon immobilisation of the G/Co_3O_4 upon screen-printed macroelectrodes (G/Co_3O_4-SPEs) the G/Co_3O_4-SPEs were found to exhibit remarkable electrocatalytic properties towards the Oxygen Reduction Reaction (OER). A detailed investigation has been carried out on the influence that the graphitization of the citric acid has, during the course of preparation of Co_3O_4, upon the G/Co_3O_4 ability to catalyse the OER in alkaline conditions (1.0 M KOH). The graphitization of citric acid ensures the uniform distribution of Co_3O_4 and enhanced conductivity with maximal exposure of active sites, which are the key parameters to delivers enhanced electrochemical activity. The G/Co_3O_4-SPEs exhibits an overpotential of 304 mV (recorded at 10 mA cm^{-2}), a Tafel slope of 110 mV dec^{-1} and remained stable in its signal output (achievable current density) at varying temperatures (5-50 ºC), and after 10 hours of chronoamperometry in 1.0 M KOH. The G/Co_3O_4-SPE's OER activity was superior to that of bulk and nano Co_3O_4. The results exhibited within this study will enable production of high-performance and environmentally benign electrocatalysts towards the OER for use within water splitting devices.

Keyword: Functionalization, Graphitic carbon, Co_3O_4, Oxygen evolution reaction, Energy storage

2. Introduction

As the economic, environmental and social impacts of anthropogenic climate change and air pollution worsen, there is an increasing impetus to make a paradigm shift within the global energy economy away from fossil fuels (FF) to low/non-polluting renewable energy sources.[1, 2] Green hydrogen produced *via* electrolysis is a promising clean energy vector/fuel. The limiting factor in the ubiquitous utilisation of green hydrogen is its cost in comparison to its FF counterparts. A major contributor to the cost of hydrogen production is the requirement for expensive noble metal catalysts (Pt, Ru and Ir based oxides),[3, 4] to overcome the large kinetic barrier associated with the oxygen evolution reaction (OER). The OER's sluggish kinetics are due to its reaction pathway having four single electron transfer steps.[5] Consequently, the synthesis of a comparatively cheap electrocatalyst, which demonstrates good structural/chemical stability, fast electrical conductivity and sufficiently lowers the OERs overpotential, is desirable.[6-9]

Co, Ni, Fe and Mn (particularly, oxides, hydroxides, oxyhydroxide, alloys and nanohybrid) have potential to be cost effective alternatives to precious metal catalysts for the OER., For instance, $La_{1-x}Sr_xCoO_3$ perovskite [10, 11], $Cu_{1-x}NNi_{3-y}$[12], sulfur doped cobalt [13], $SrCo_{0.4}Fe_{0.2}W_{0.4}O_{3-\delta}$ [14], $CoMn_2O_4$ embedded in MnOOH [15], graphene decorated $Co(OH)_2$ [16], Co_3O_4 [17], Ag doped Co_3O_4 [18], RuO_2/Co_3O_4 [19], $Ni(OH)_2$ [20], W doped Ni-Co phosphides [21], MoCoNiS [22] have been employed as electrocatalyst for OER. However, whilst enabling the OER to occur at low overpotentials they typically have had limited utilization as the anodic catalyst material with operational electrolysers due to their low number of active sites, poor electronic conductivity and poor stability within alkaline conditions. Nevertheless, the catalytic performance of the electrocatalyst towards OER has been greatly enhanced by tuning the electronic structure[23-27], nanostructuring/nanoscaling,[28] and creating oxygen defects [29, 30]. However, they still do not display sufficient energy conversion for practical/industrial applications.

Recent studies have doped transition metal catalysts onto carbon/graphene/carbon nanotube frameworks to enhance their performance towards the OER [31]. For instance Suryanto *et al.*[32] prepared a Co_3O_4/graphene composite by layer-by-layer electodeposition onto an indium tin oxide (ITO) substrate. This Co_3O_4/graphene composite electrode was then explored towards the OER where it yielded a remarkable overpotential of 360 mV (recorded at 10 mA cm^{-2}). This

overpotential was significantly lower and therefore more beneficial than the Co_3O_4 or the graphene alone. Despite the catalyst described above as well as many of the catalysts described within Table S1 showing efficient OER catalysis, the reported synthesis methods are often expensive, time consuming and complex, which significantly detracts from the catalysts desirability within industry.

In order to produce a cost effective transition metal OER catalyst that benefits from a carbon support framework but does not rely upon a time consuming and costly synthesis technique we propose a novel *in situ* addition and optimization of the highly conductive graphitic carbon into cobalt oxide *via* a simple citrate-nitrate decomposition approach. We then explore the synthesized catalysts towards the OER. This entails a simple synthetic protocol that has been proposed to synthesize graphitic carbon functionalized Co_3O_4. The graphitization of citric acid during the preparation of Co_3O_4 ensures the uniform distribution and exposure of active sites. Furthermore, the degree graphitization of citric acid during the preparation of Co_3O_4 has been optimized to enhance the electroconductivity and exposure of active sites; which in turn increases its ability to catalyse the OER. Impressively, the graphitic carbon functionalized Co_3O_4 is recorded as achieving a current density of 10 mA cm^{-2} at low overpotential of 304 mV, which outperforms most traditional RuO_2 and IrO_2 catalysts.

3. RESULT AND DISCUSSION

3.1. Co_3O_4/graphite synthesis procedure

The synthesis technique utilised to fabricate the Co_3O_4/graphite (G/Co_3O_4) electrocatalyst is fully described within the supporting information (SI) with a summary given below. Graphitic carbon functionalized Co_3O_4 (G/Co_3O_4) was synthesized through a simple and rapid decomposition of the aqueous mixture of citric acid and cobalt nitrate. In a typical synthesis, 0.171 mM of cobalt nitrate hexahydrate was dissolved in 100 mL beaker containing 10 mL of deionized water and stirred until the metal nitrate dissolves completely. To the resulting solution, 0.01 M of citric acid was added and stirring was continued for another 10 minutes to get a homogeneous solution. Then, the vessel containing cobalt nitrate and citric acid mixture was kept in a preheated muffle furnace maintained at 500 ºC. The decomposition of the mixture starts after evaporating water and leads to the G/Co_3O_4 wherein the overall process takes about 4 minutes. Then, the reaction vessel was taken out from the preheated muffle furnace and allowed to cool. Finally, the G/Co_3O_4 was crushed in a mortar and pestle and used for further study. The schematic representation of the preparation of graphitic carbon functionalized Co_3O_4 is shown in Figure 1.

3.2. Physicochemical Characterisation

In order to determine the quality and purity of the G/Co_3O_4 electrocatalyst, a thorough physicochemical characterisation was performed. This included Fourier Transform Infrared Spectroscopy (FTIR), Scanning Electron Microscopy (SEM), Transmission Electron Microscopy (TEM) / High Resolution Electron Microscopy (HRTEM) and X-ray diffraction (XRD). Interested readers are directed towards the SI for specific details on the FTIR, TEM, SEM and XRD equipment utilised.

XRD identified the characteristic diffraction peaks for Co_3O_4 pattern (Figure 2(A)) at 30.77°, 36.27°, 38.16°, 44.35°, 55.18°, 58.96° and 64.98°, which can be assigned to the crystalline planes of (220), (311), (222), (400), (422), (511) and (440), respectively indicating the formation of pure cubic Co_3O_4 [33]. The average crystalline size calculated for the (*311*) diffraction peak is found to be 17 nm. This small crystallite size of the synthesized Co_3O_4 was evidenced by the significant broadening of the diffraction peaks. The formation of Co_3O_4 was also reflected in the FTIR spectrum, shown in Figure 2(B), where the stretching vibrations appeared in the range of 400−700

cm^{-1} corresponding to metal−oxygen bonding. Particularly, the stretching vibration at 657 cm^{-1} corresponds to the Co−O where Co^{2+} is tetrahedrally coordinated. Another visible peak at 567 cm^{-1} corresponded to the Co−O where Co^{3+} ($3d^6$) is octahedrally coordinated, confirming the formation of cubic Co_3O_4 [34, 36-39]. The TEM image of the G/Co_3O_4 shown in Figure 3(A) indicated the presence well dispersed uniform discreet nanoparticles. Further, the TEM image shown in Figure 3(B) revealed the electrical wiring of graphitic carbon with the Co_3O_4 particles. This significantly enhanced the electronic conductivity, which is a crucial parameter to achieve high efficiency of OER. The inter-planar distance of 0.284 nm observed in the HRTEM presented in Figure 3(C) corresponded to the (220) plane of Co_3O_4, which confirmed the presence Co_3O_4 on graphitic carbon.

The coexistence of cobalt nitrate and citric acid produced graphitic functionalised carbon. This was confirmed from the FTIR and Raman spectrum shown in Figure 2(B) and 2(C) respectively. Initially the citric acid underwent thermal decomposition at 500 °C for 4 minutes resulting in graphitic carbon [40], confirmed by FTIR (Figure S1(A)). The morphology of the graphitic carbon prepared by the decomposition of citric acid alone exhibited a layered structure (Figure S1(B)). Further, the high degree graphitization of citric acid in Co_3O_4 was evidenced by the intensities of the D and G bands in the FTIR spectrum; where the D and G bands corresponded to the disordered carbon (sp^3 carbon) and ordered graphitic carbon (sp^2 carbon) respectively [41]. The ratio of I_D/I_G, deduced from the IR spectrum, was found to be 0.9745 for G/Co_3O_4. The effect of the degree of graphitization on the electronic conductivity was further studied by electrochemical impedance analysis shown in Figure 4. In order to explore the effect of modifying SPEs with the Co_3O_4 based electrocatalysts had upon the charge transfer resistance (Ω) electrochemical impedance spectroscopy (EIS) was performed. Note that upon immobilization of the G/Co_3O_4 upon SPEs the subsequent electrode is denoted as G/Co_3O_4-SPEs.

The G/Co_3O_4 (prepared in presence of citric acid at 500 ºC for 4 minutes) exhibited the least charge transfer resistance of 143 Ω ±3.20. This value was significantly smaller than the charge transfer resistance displayed by the nano Co_3O_4 prepared (Figure S2, supporting information) by the decomposition of cobalt nitrate alone at 500 ºC for 4 minutes without citric acid (325.3 Ω ± 1.85%), and graphitic carbon (156 Ω) prepared from the decomposition of citric acid alone under the same conditions. Bulk Co_3O_4 was prepared using citric acid and cobalt nitrate at 500 ºC for 8 hours

(Figure S3, supporting information). The morphology of the bulk Co_3O_4 exhibited highly agglomerated particles (Figure S4(A)). Thus, the prepared bulk Co_3O_4 exhibited very high charge transfer resistance of 868.0 Ω ± 0.69%. The high resistivity may be due to the bigger crystallite size (52 nm) of Co_3O_4 and absence of graphitic carbon revealed by FTIR spectrum, shown in Figure S4(B), where the absence of the D and G band indicated that decomposition time played an important role in retaining the graphitic carbon. It is worth note that the charge transfer resistance increases with increase in crystallite size. Thus, the presence of graphitic carbon and small crystallite size of Co_3O_4 endows the enhanced electronic conductivity and thereby made it favorable to exhibit improved OER catalytic performance.

3.3. Electrochemical Characterisation

The G/Co_3O_4 was drop-cast onto screen-printed macroelectrodes (G/Co_3O_4-SPEs) (see Figure S5) and tested towards the OER in 1.0 M KOH solution (details given in supporting information). As shown in Figure S6, a distinct pair of redox peaks appeared in the cyclic voltammogram (CV) during anodic and cathodic sweeps, where the oxidation peak at + 0.37 V and cathodic peak at + 0.31 V corresponded to the Co(III)→Co(IV) transition [39]. Scan rate studies are presented in Figure S7. Further, the sudden and sharp increase in anodic current after Co(III)→Co(IV) transition signified the catalytic activity of G/Co_3O_4 towards OER [23, 24]. The catalytic activity of the G/Co_3O_4 towards OER was evaluated by using linear sweep voltammetry (LSV). The G/Co_3O_4-SPEs exhibited an oxidation peak at 1.32 V *vs.* RHE (Figure 5) due to the oxidation of Co(III) to Co(IV),[42] this is followed by a sharp increase in anodic current, which started at 1.40 V *vs.* RHE (Figure S8) and reached a current density of 10 mA cm^{-2} by 1.52 V ± 0.17% *vs.* RHE. It is important to note that the generation of O_2 bubbles, upon the electrode surface, was visible to the naked eye. The overpotential required to reach a current density of 10 mA cm^{-2} was found to be 304 mV as shown in the Figure S8 (B). This was less electropositive than the overpotential value of 340 mV and 350 mV observed for IrO_2 and RuO_2 respectively [43]. Note that Figure S10 shows the obtained CV scans for a RuO_2 electrode and bare/unmodified SPEs. Further, the OER performance of G/ Co_3O_4 was compared with nano Co_3O_4 and bulk Co_3O_4. Interestingly, the oxidation peak (at *ca.* 1.3 V *vs.* RHE) observed for G/Co_3O_4 shown in Figure 5, shifts positively compared to the oxidation peaks for nano Co_3O_4 and bulk Co_3O_4. This positive shift indicated the enhanced OER activity [44]. The observed result was similar to the report documented for the Fe

doped Ni(oxy)hydroxide where Fe doping lead to a positive shift and it exhibited enhanced OER activity [45, 46]. Further, as shown in the Figure S8(B), the overpotential required to reach 10 mA cm^{-2} for nano Co_3O_4 and bulk Co_3O_4 were found to be 315 mV and 345 mV (Detailed graphs are provided in Figure S8(A) and (B), respectively. The absence of the synergetic effect of graphitic carbon and active Co_3O_4 (confirmed from the FTIR spectrum of Figures S1, Figures S4 and Figures S9) lead to larger overpotentials compared to the G/Co_3O_4. The bulk Co_3O_4 displayed a relatively large overpotential of 345 mV, this is likely due to the synthesis procedure involving a long exposure (8 hour) of the aqueous mixture of cobalt nitrate and citric acid (at 500 ºC), which resulted in the removal of graphitic carbon, as CO_2. This process caused the formation of Co_3O_4 with larger particle sizes as a result of the sintering effect, which was confirmed *via* XRD (Figure S11) and SEM analysis. Whereas, the nano Co_3O_4 prepared using aqueous cobalt nitrate alone required a comparatively low ovepotential of 315 mV as compared to graphitic carbon and bulk Co_3O_4. This may be due to the small crystallite size of Co_3O_4 (confirmed by the powder XRD pattern shown in Figure S12, leading to a larger number of exposed electrocatalytic sites available, (the crystallite size was found to be *ca*. 23 nm). The results above demonstrate that the small crystallite size and presence of graphitic carbon significantly influenced the OER performance of Co_3O_4. Thus, G/Co_3O_4 together with small crystallite size improved the OER catalysis of Co_3O_4 particles. The Co_3O_4 OER electrocatalyst that displayed the least electropositive overpotential was the G/Co_3O_4.

The lowest overpotential observed for G/Co_3O_4-SPEs is well supported electrochemically active surface area (ECSA) measurements, shown in Figure S13. The observed ECSA values for Co3O4 samples were summarized in the table 1 where G/Co_3O_4-SPE exhibits highest ECSA of 892.5 cm^2. The observed tafel slope (Figure 6) between 110 and 140 mV dec^{-1} suggested that the –OH adsorption step was the rate determining step [43, 47] according to the following equation[48-50] shown in scheme 1. The observed slope was lower than the valued obtained by RuO_2 (169 mV dec^{-1}), and Pt/C (223 mV dec^{-1}). This low Tafel slope of 110 mV dec^{-1} demonstrated improved oxygen evolution kinetics on G/Co_3O_4. The improved OER is attributed to the synergic effect of high enhanced conductivity with small crystallite size and good dispersion of active sites in the graphitic carbon [42]. In order to determine the OER activity of the G/Co_3O_4 on a per active site basis, OER turnover frequency (TOF) values were calculated (see SI for TOF calculation). The G/Co_3O_4 produced a TOF value of 0.03743 s^{-1} at 304 mV, which is 2.0 and 187 times higher than

the previously reported Co_3O_4 (0.0187 s^{-1} at 328 mV) and $P_{8.6}$-Co_3O_4 nano-fibres (2.03 x 10^{-4} s^{-1} at 350 mV).[51] The G/Co_3O_4 exhibited a Tafel slope of 110 mV dec^{-1} as shown in Figure 6, which is much lower than the Tafel slope values observed for nano Co_3O_4 (130 mV dec^{-1}) and bulk Co_3O_4 (140 mV dec^{-1}).

In order to examine the signal output stability of G/Co_3O_4-SPEs chronoamperometric was performed. A voltage of + 0.7 V was applied to a G/Co_3O_4-SPEs (in 1.0 M KOH) for 10 hours (See Figure S14). There was an observed slight increase in current in the beginning and thereafter it remains almost constant with ~95% relative current retention, indicating active sites were continuously regenerated [52]. The slight increase in the current may be due to the improved wettability/activation of the electrode. The catalytic performance of G/Co_3O_4 in 1 M KOH at different temperatures is shown in Figure 7(A-C). Where the potential required to deliver 10 mA cm^{-2} was found to be 1.56, 1.52, 1.50 and 1.48 V *vs.* RHE respectively at 278, 298, 308 and 323 K (Figure 7(A)), indicating that the increase of temperature leads to a decrease in overpotential (Figure 7(B)). Additionally, higher OER current density could be achieved at a lower overpotential manifesting in the faster the reaction rate at higher temperature, which is consistent with the Arrehenius' law. Further, monotonic increase of OER performance with the temperature was confirmed by the linear relationship of η and 1/T [53].

4. Conclusions

A novel, facile protocol for the synthesis of highly active Co_3O_4 functionalized with graphitic carbon (G/Co_3O_4) has been produced. This methodology is a scalable and rapid approach that eliminates the complexity of handling the reaction. The G/Co_3O_4 exhibited a uniform distribution of active sites, enhanced conductivity and small crystallite size. These factors improved the catalysts kinetic performance toward water splitting, delivering a low overpotential (304 mV to produce 10 mA cm^{-2}) which is much lower than the bulk material. Tafel analysis of the material produced a slope of 110 mV dec^{-1} and the system delivered a stable signal output at various temperatures after 10 h. The performance of the G/Co_3O_4 toward the OER was found to be superior to the bulk material and nano Co_3O_4, as well as comparable to that of reported OER electrocatalyst RuO_2. Due to the performance and facile synthetic route, this electrocatalyst lends itself to the mass production of a high-performance and environmentally benign electrocatalyst for the OER in water splitting devices.

Acknowledgements

SA (Ashoka S) thanks Science and Engineering Research Board (SERB, Project No. ECR/2017/000743) Government of India, for financial support to carry out this research work. Funding from the Engineering and Physical Sciences Research Council (Reference: EP/P007767/1 and EP/N0011877/1), British Council Institutional Grant Link (No. 172726574) is acknowledged. The Manchester Fuel Cell Innovation Centre is funded by the European Regional Development Fund.

5. References

[1] Manzoor ZM, Thimmappa R, Devendrachari MC, Kottaichamy AR, Shafi SP, Varhade S, et al. Fuel Exhaling Fuel Cell. J Phys Chem Lett. 2018;9:388-92.
[2] Dargily NC, Thimmappa R, Bhat ZM, Devendrachari MC, Kottaichamy AR, Gautam M, et al. A Rechargeable Hydrogen Battery. J Phys Chem Lett. 2018;9:2492-7.
[3] Park S, Shao Y, Liu J, Wang Y. Oxygen electrocatalysts for water electrolyzers and reversible fuel cells: status and perspective. Energy Environ Sci. 2012;5:9331-44.
[4] Reier T, Oezaslan M, Strasser P. Electrocatalytic Oxygen Evolution Reaction (OER) on Ru, Ir, and Pt Catalysts: A Comparative Study of Nanoparticles and Bulk Materials. ACS Catalysis. 2012;2:1765-72.
[5] Tahir M, Pan L, Idrees F, Zhang X, Wang L, Zou J-L, et al. Electrocatalytic oxygen evolution reaction for energy conversion and storage: A comprehensive review. Nano Energy. 2017;37:136-57.
[6] Li X, Yang X, Xue H, Pang H, Xu Q. Metal–organic frameworks as a platform for clean energy applications. EnergyChem. 2020;2:100027.
[7] Li D, Xu H-Q, Jiao L, Jiang H-L. Metal-organic frameworks for catalysis: State of the art, challenges, and opportunities. EnergyChem. 2019;1:100005.
[8] Zheng S, Li B, Tang Y, Li Q, Xue H, Pang H. Ultrathin nanosheet-assembled $[Ni_3(OH)_2(PTA)_2(H_2O)_4]\cdot 2H_2O$ hierarchical flowers for high-performance electrocatalysis of glucose oxidation reactions. Nanoscale. 2018;10:13270-6.
[9] Li X, Xue H, Pang H. Facile synthesis and shape evolution of well-defined phosphotungstic acid potassium nanocrystals as a highly efficient visible-light-driven photocatalyst. Nanoscale. 2017;9:216-22.
[10] Cheng X, Fabbri E, Nachtegaal M, Castelli IE, El Kazzi M, Haumont R, et al. Oxygen Evolution Reaction on $La1–xSrxCoO_3$ Perovskites: A Combined Experimental and Theoretical Study of Their Structural, Electronic, and Electrochemical Properties. Chemistry of Materials. 2015;27:7662-72.
[11] Wei C, Feng Z, Baisariyev M, Yu L, Zeng L, Wu T, et al. Valence Change Ability and Geometrical Occupation of Substitution Cations Determine the Pseudocapacitance of Spinel Ferrite XFe_2O_4 (X = Mn, Co, Ni, Fe). Chemistry of Materials. 2016;28:4129-33.
[12] Zhu Y, Chen G, Zhong Y, Chen Y, Ma N, Zhou W, et al. A surface-modified antiperovskite as an electrocatalyst for water oxidation. Nature Communications. 2018;9:2326.
[13] Al-Mamun M, Zhu Z, Yin H, Su X, Zhang H, Liu P, et al. The surface sulfur doping induced enhanced performance of cobalt catalysts in oxygen evolution reactions. Chemical Communications. 2016;52:9450-3.
[14] Chen G, Hu Z, Zhu Y, Chen Z-G, Zhong Y, Lin H-J, et al. Ultrahigh-performance tungsten-doped perovskites for the oxygen evolution reaction. Journal of Materials Chemistry A. 2018;6:9854-9.
[15] Panapitiya G, Wang H, Chen Y, Hussain E, Jin R, Lewis JP. Structural and catalytic properties of the Au25−xAgx(SCH3)18 (x = 6, 7, 8) nanocluster. Physical Chemistry Chemical Physics. 2018;20:13747-56.
[16] Cai Z, Bi Y, Hu E, Liu W, Dwarica N, Tian Y, et al. Single-Crystalline Ultrathin Co_3O_4 Nanosheets with Massive Vacancy Defects for Enhanced Electrocatalysis. Advanced Energy Materials. 2018;8:1701694.
[17] Yan K-L, Qin J-F, Lin J-H, Dong B, Chi J-Q, Liu Z-Z, et al. Probing the active sites of Co_3O_4 for the acidic oxygen evolution reaction by modulating the Co^{2+}/Co^{3+} ratio. Journal of Materials Chemistry A. 2018;6:5678-86.
[18] Yan K-L, Chi J-Q, Xie J-Y, Dong B, Liu Z-Z, Gao W-K, et al. Mesoporous Ag-doped Co_3O_4 nanowire arrays supported on FTO as efficient electrocatalysts for oxygen evolution reaction in acidic media. Renewable Energy. 2018;119:54-61.
[19] Guo B-Y, Zhang X-Y, Ma X, Chen T-S, Chen Y, Wen M-L, et al. RuO_2/Co_3O_4 Nanocubes based on Ru ions impregnation into prussian blue precursor for oxygen evolution. International Journal of Hydrogen Energy. 2020;45:9575-82.

[20] Anantharaj S, Karthik PE, Kundu S. Petal-like hierarchical array of ultrathin $Ni(OH)_2$ nanosheets decorated with $Ni(OH)_2$ nanoburls: a highly efficient OER electrocatalyst. Catalysis Science & Technology. 2017;7:882-93.
[21] Lu S-S, Zhang L-M, Dong Y-W, Zhang J-Q, Yan X-T, Sun D-F, et al. Tungsten-doped Ni–Co phosphides with multiple catalytic sites as efficient electrocatalysts for overall water splitting. Journal of Materials Chemistry A. 2019;7:16859-66.
[22] Qin J-F, Yang M, Chen T-S, Dong B, Hou S, Ma X, et al. Ternary metal sulfides MoCoNiS derived from metal organic frameworks for efficient oxygen evolution. International Journal of Hydrogen Energy. 2020;45:2745-53.
[23] Cheng X, Fabbri E, Nachtegaal M, Castelli IE, Kazzi ME, Haumont R, et al. Oxygen Evolution Reaction on $La_{1-x}Sr_xCoO_3$ Perovskites: A Combined Experimental and Theoretical Study of Their Structural, Electronic, and Electrochemical Properties. Chem Mater. 2015;27:7662-72.
[24] Wei C, Feng Z, Baisariyev M, Yu L, Zeng L, Wu T, et al. Valence Change Ability and Geometrical Occupation of Substitution Cations Determine the Pseudocapacitance of Spinel Ferrite XFe_2O_4 (X = Mn, Co, Ni, Fe). Chem Mater. 2016;28:4129-33.
[25] Zhu Y, Chen G, Zhong Y, Chen Y, Ma N, Zhou W, et al. A surface-modified antiperovskite as an electrocatalyst for water oxidation. Nat Commun. 2018;9:2326.
[26] Al-Mamun M, Zhu Z, Yin H, Su X, Zhang H, Liu P, et al. The surface sulfur doping induced enhanced performance of cobalt catalysts in oxygen evolution reactions. Chem Commun. 2016;52:9450-3.
[27] Chen G, Hu Z, Zhu Y, Chen Z-G, Zhong Y, Lin H-J, et al. Ultrahigh-performance tungsten-doped perovskites for the oxygen evolution reaction. J Mater Chem A. 2018;6:9854-9.
[28] Panapitiya G, Wang H, Chen Y, Hussain E, Jin R, Lewis JP. Structural and catalytic properties of the $Au_{25-x}Ag_x(SCH_3)_{18}$ (x = 6, 7, 8) nanocluster. Phys Chem Chem Phys. 2018;20:13747-56.
[29] Cai Z, Bi Y, Hu E, Liu W, Dwarica N, Tian Y, et al. Single-Crystalline Ultrathin Co_3O_4 Nanosheets with Massive Vacancy Defects for Enhanced Electrocatalysis. Adv Energy Mater. 2018;8:1701694.
[30] Zhang T, Wu M-Y, Yan D-Y, Mao J, Liu H, Hu W-B, et al. Engineering oxygen vacancy on NiO nanorod arrays for alkaline hydrogen evolution. Nano Energy. 2018;43:103-9.
[31] Ashok A, Kumar A, Matin MA, Tarlochan F. Synthesis of Highly Efficient Bifunctional Ag/Co_3O_4 Catalyst for Oxygen Reduction and Oxygen Evolution Reactions in Alkaline Medium. ACS Omega. 2018;3:7745-56.
[32] Suryanto BHR, Lu X, Zhao C. Layer-by-layer assembly of transparent amorphous Co3O4 nanoparticles/graphene composite electrodes for sustained oxygen evolution reaction. J Mater Chem A. 2013;1:12726-31.
[33] Zhang L, He W, Xiang X, Li Y, Li F. Roughening of windmill-shaped spinel Co_3O_4 microcrystals grown on a flexible metal substrate by a facile surface treatment to enhance their performance in the oxidation of water. RSC Adv. 2014;4:43357-65.
[34] Maruthapandian V, Mathankumar M, Saraswathy V, Subramanian B, Muralidharan S. Study of the Oxygen Evolution Reaction Catalytic Behavior of $Co_xNi_{1-x}Fe_2O_4$ in Alkaline Medium. ACS Applied Materials & Interfaces. 2017;9:13132-41.
[35] Farhadi S, Safabakhsh J, Zaringhadam P. Synthesis, characterization, and investigation of optical and magnetic properties of cobalt oxide (Co_3O_4) nanoparticles. JNSC. 2013;3:69.
[36] Farhadi S, Safabakhsh J, Zaringhadam P. Synthesis, characterization, and investigation of optical and magnetic properties of cobalt oxide (Co_3O_4) nanoparticles. Journal of Nanostructure in Chemistry. 2013;3:69.
[37] Hoekstra J, Beale AM, Soulimani F, Versluijs-Helder M, Geus JW, Jenneskens LW. Base Metal Catalyzed Graphitization of Cellulose: A Combined Raman Spectroscopy, Temperature-Dependent X-ray Diffraction and High-Resolution Transmission Electron Microscopy Study. The Journal of Physical Chemistry C. 2015;119:10653-61.

[38] Li L, Guo Z, Du A, Liu H. Rapid microwave-assisted synthesis of Mn_3O_4–graphene nanocomposite and its lithium storage properties. Journal of Materials Chemistry. 2012;22:3600-5.
[39] Devaguptapu SV, Hwang S, Karakalos S, Zhao S, Gupta S, Su D, et al. Morphology Control of Carbon-Free Spinel $NiCo_2O_4$ Catalysts for Enhanced Bifunctional Oxygen Reduction and Evolution in Alkaline Media. ACS Applied Materials & Interfaces. 2017;9:44567-78.
[40] Hoekstra J, Beale AM, Soulimani F, Versluijs-Helder M, Geus JW, Jenneskens LW. Base Metal Catalyzed Graphitization of Cellulose: A Combined Raman Spectroscopy, Temperature-Dependent X-ray Diffraction and High-Resolution Transmission Electron Microscopy Study. J Phys Chem C. 2015;119:10653-61.
[41] Li L, Guo Z, Du A, Liu H. Rapid microwave-assisted synthesis of Mn_3O_4–graphene nanocomposite and its lithium storage properties. J Mater Chem. 2012;22:3600-5.
[42] Burke LD, Lyons ME, Murphy OJ. Formation of hydrous oxide films on cobalt under potential cycling conditions. J Electroanal Chem Interfacial Electrochem. 1982;132:247-61.
[43] Tahir M, Pan L, R. Zhang, Wang Y-C, Shen G, Aslam I, et al. High-Valence-State NiO/Co_3O_4 Nanoparticles on Nitrogen-Doped Carbon for Oxygen Evolution at Low Overpotential. ACS Energy Lett. 2017;2:2177-82.
[44] Fu G, Wen X, Xi S, Chen Z, Li W, Zhang J-Y, et al. Tuning the Electronic Structure of NiO via Li Doping for the Fast Oxygen Evolution Reaction. Chem Mater. 2019;31:419-28.
[45] Trotochaud L, Young SL, Ranney JK, Boettcher SW. Nickel–Iron Oxyhydroxide Oxygen-Evolution Electrocatalysts: The Role of Intentional and Incidental Iron Incorporation. J Am Chem Soc. 2014;136:6744-53.
[46] Klaus S, Louie MW, Trotochaud L, Bell AT. Role of Catalyst Preparation on the Electrocatalytic Activity of Ni1–xFexOOH for the Oxygen Evolution Reaction. J Phys Chem C. 2015;119:18303-16.
[47] Song F, Hu X. Exfoliation of layered double hydroxides for enhanced oxygen evolution catalysis. Nat Commun. 2014;5:4477.
[48] R. Wei R, M. Fang M, G. Dong G, C. Lan C, L. Shu L, Zhang H, et al. High-Index Faceted Porous Co_3O_4 Nanosheets with Oxygen Vacancies for Highly Efficient Water Oxidation. ACS Appl Mater Interfaces. 2018;10:7079-86.
[49] Ray C, Lee SC, Jin B, Kundu A, Park JH, Jun SC. Stacked Porous Iron-Doped Nickel Cobalt Phosphide Nanoparticle: An Efficient and Stable Water Splitting Electrocatalyst. ACS Sustainable Chemistry & Engineering. 2018;6:6146-56.
[50] Zhang Q, Yan D, Nie Z, Qiu X, Wang S, Yuan J, et al. Iron-Doped NiCoP Porous Nanosheet Arrays as a Highly Efficient Electrocatalyst for Oxygen Evolution Reaction. ACS Applied Energy Materials. 2018;1:571-9.
[51] Chou NH, Ross PN, Bell AT, Tilley TD. Comparison of Cobalt-based Nanoparticles as Electrocatalysts for Water Oxidation. ChemSusChem. 2011;4:1566-9.
[52] Singh DK, Chakraborty S, Saha A, Sampath S, Eswaramoorthy M. Pick a Wick: A Simple, Ultrafast Combustion Synthesis of Co_3O_4 Dispersed Carbon for Enhanced Oxygen Evolution Kinetics. ACS Appl Energy Mater. 2018;1:4448-52.
[53] Zhang G, Wang H, Yang J, Zhao Q, Yang L, Tang H, et al. Temperature Effect on Co-Based Catalysts in Oxygen Evolution Reaction. Inorg Chem. 2018;57:2766-72.

Scheme 1. Schematic representation of the electrochemical water splitting into molecular oxygen and hydrogen on graphitic carbon functionalized M (M = Co_3O_4).

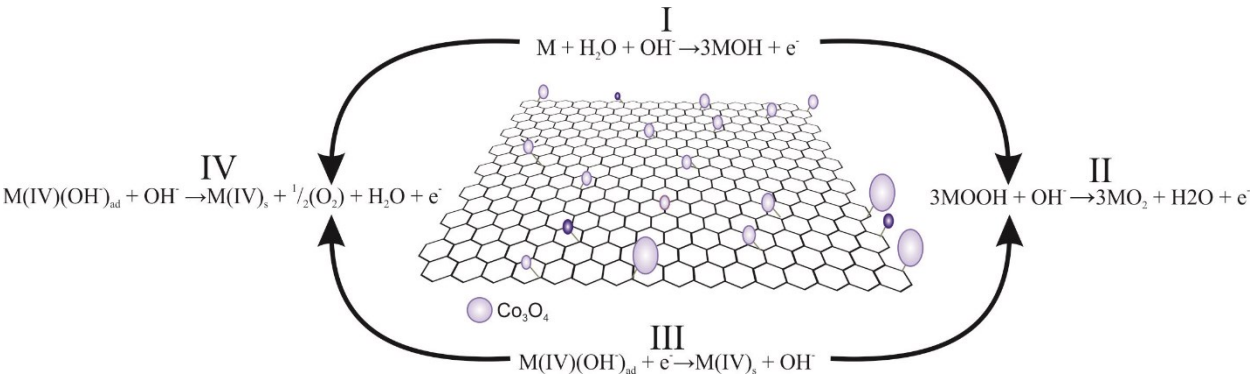

Figure 1. Schematic representation of the preparation of graphitic carbon functionalized Co_3O_4 using aqueous mixture of citric acid and cobalt nitrate at 500 ºC for 4 minutes.

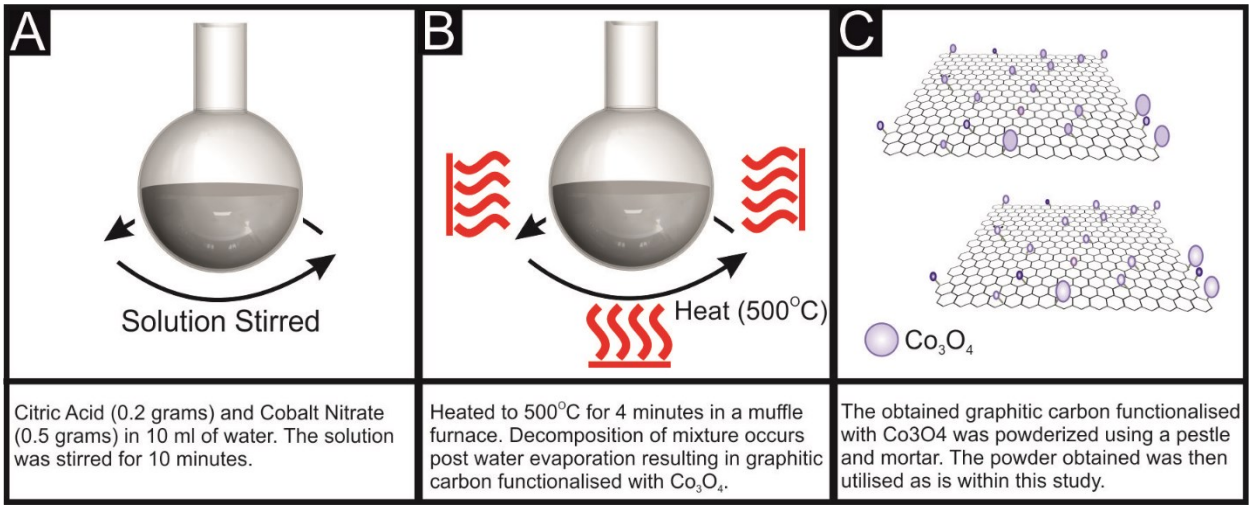

Figure 2. (A) Powder XRD pattern and (B) FTIR and (C) Raman spectrum of the graphitic carbon functionalized Co_3O_4 prepared by the citrate-nitrate decomposition of aqueous mixture of cobalt nitrate and citric acid at 500 ºC for 4 minutes.

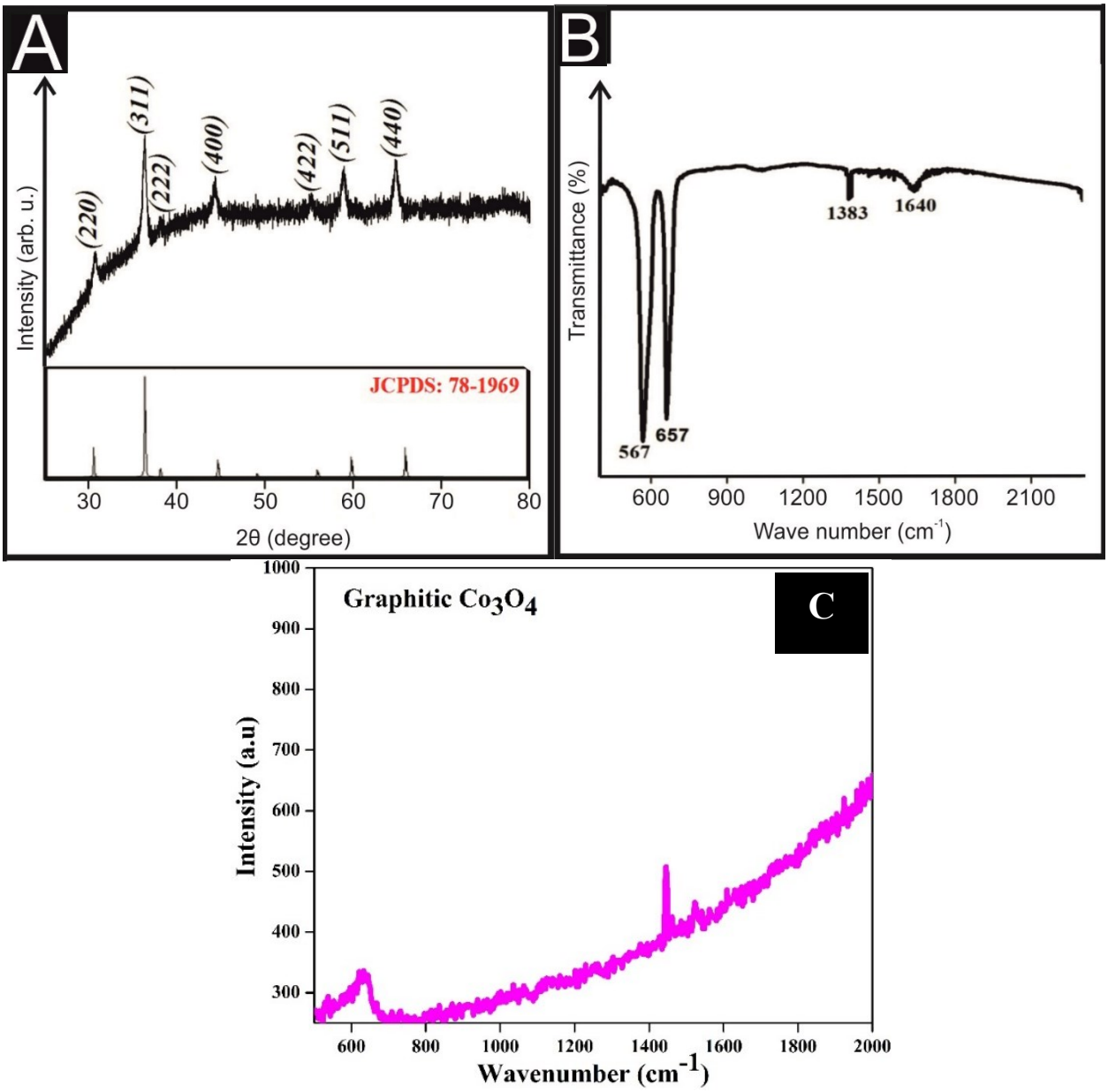

Figure 3. (A) and (B) TEM image and (C) HRTEM image of the graphitic carbon functionalized Co_3O_4 prepared by the citrate-nitrate decomposition of aqueous mixture of cobalt nitrate and citric acid at 500 ºC for 4 minutes.

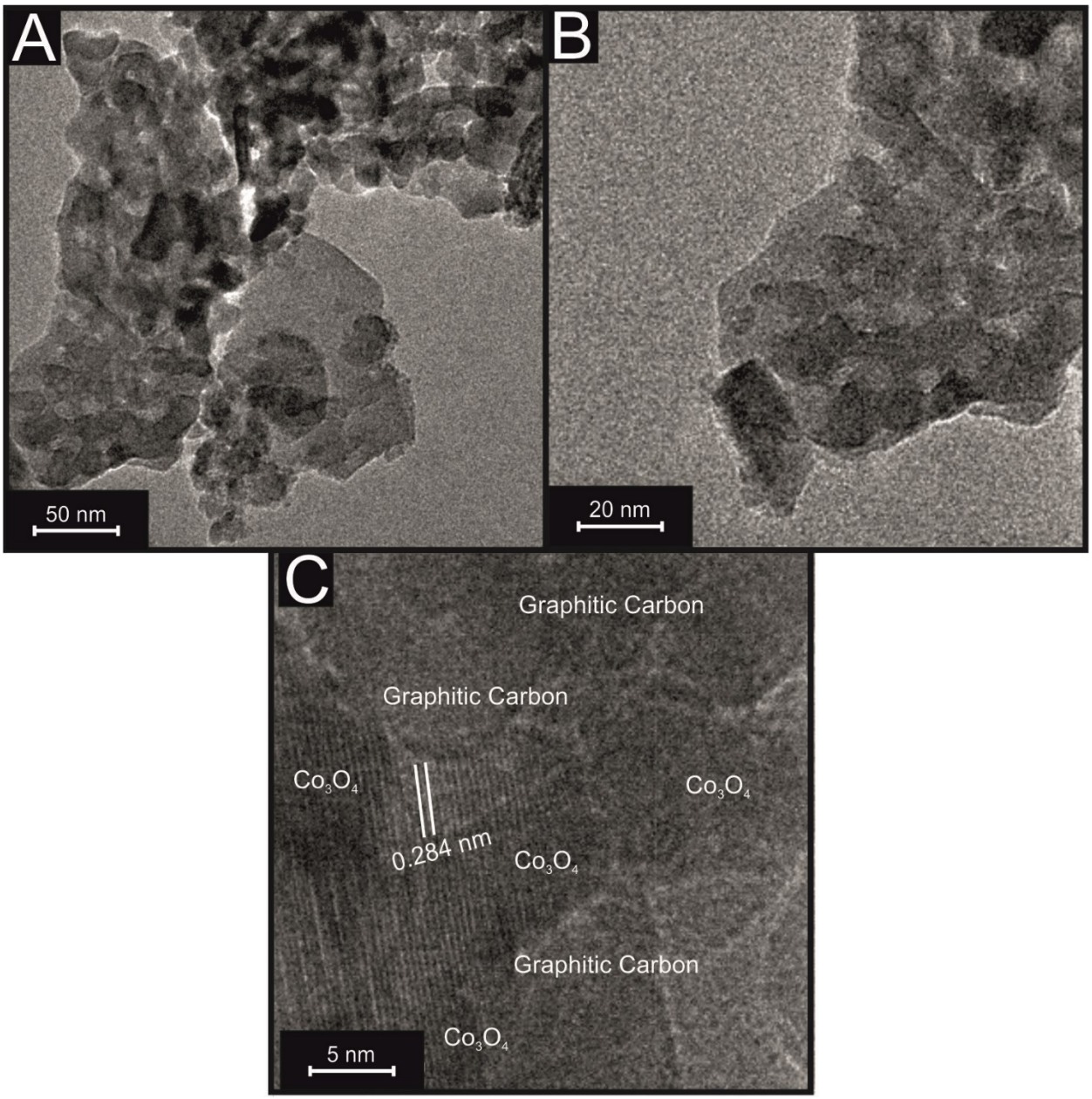

Figure 4. Electrochemical impedance spectrum of graphitic carbon functionalized Co_3O_4 (black), bulk Co_3O_4 (red), Co_3O_4 prepared without citric acid (blue) and carbon prepared using citric acid alone. Impedance spectrum was carried out in 1.0 M KOH solution in the frequency range 0.01 Hz to 100 kHz.

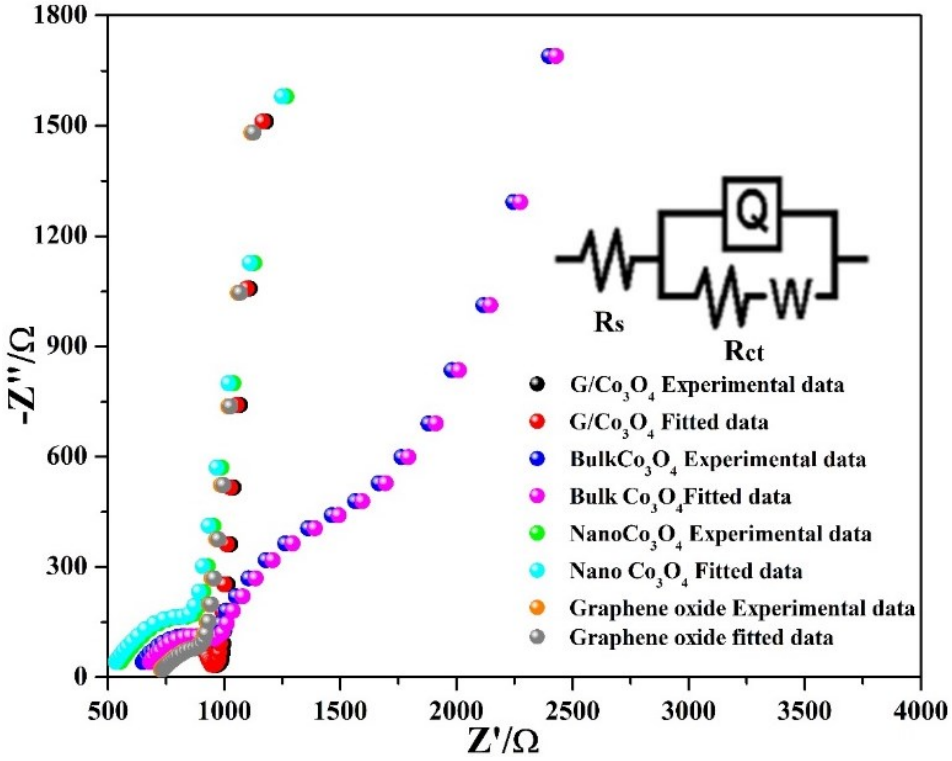

Figure 5. Linear sweep voltammetry showing the OER activity of the G/Co_3O_4 (black line), bulk Co_3O_4 (red line) and nano Co_3O_4 (blue line) deposited upon a graphitic screen-printed electrode. Solution composition: 1.0 M KOH; Scan rate: 5 mVs^{-1} (*vs*. RHE).

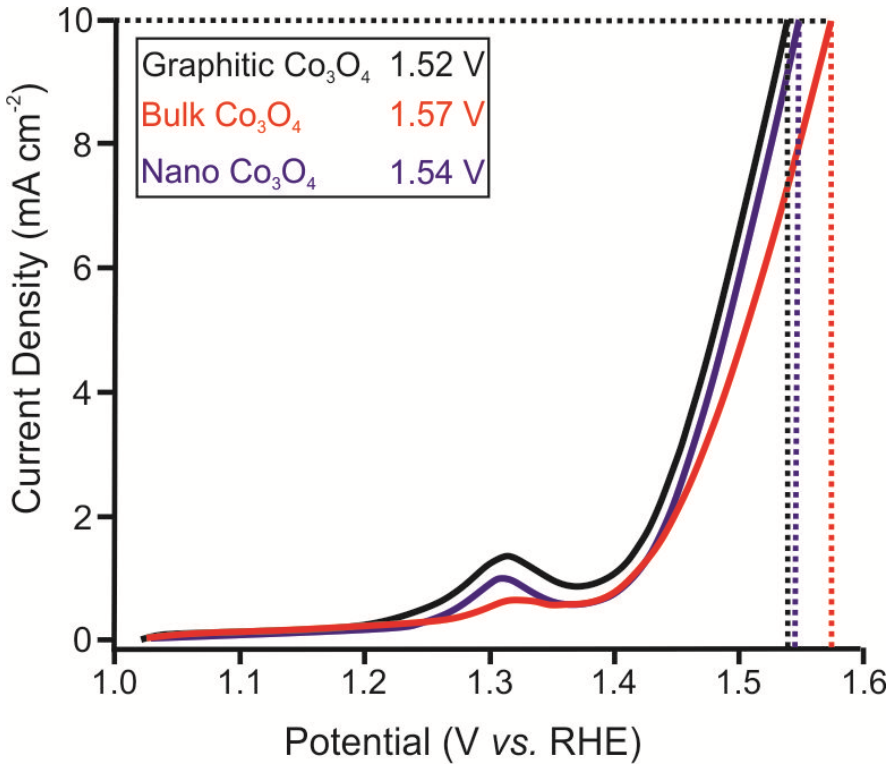

Figure 6. Tafel plots derived from the Faradaic Regions of the LSVs in Figure 5.

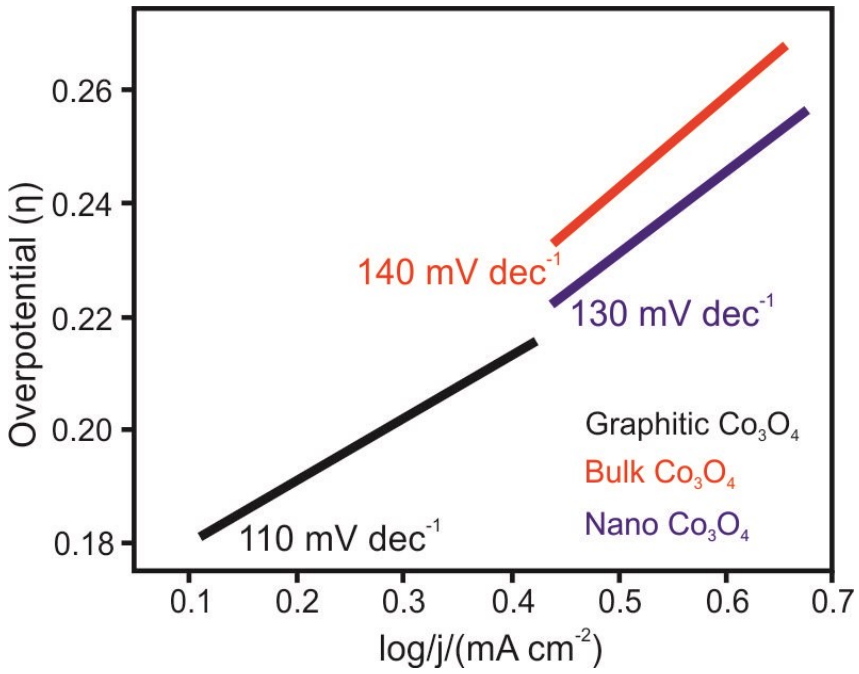

Figure 7. (A) Linear sweep voltammetry of unmodified and various modified electrodes showing OER activity of the G/Co_3O_4 (using a graphitic screen-printed electrode as an underlying support electrode), at 5 ºC 25 ºC, 35 ºC and 50 ºC. Solution composition: 1.0 M KOH; Scan rate: 5 mVs^{-1} (*vs*. RHE). (B) Linear plot showing the correlation between the obtained OER overpotential for the G/Co_3O_4 against 1/T (K).

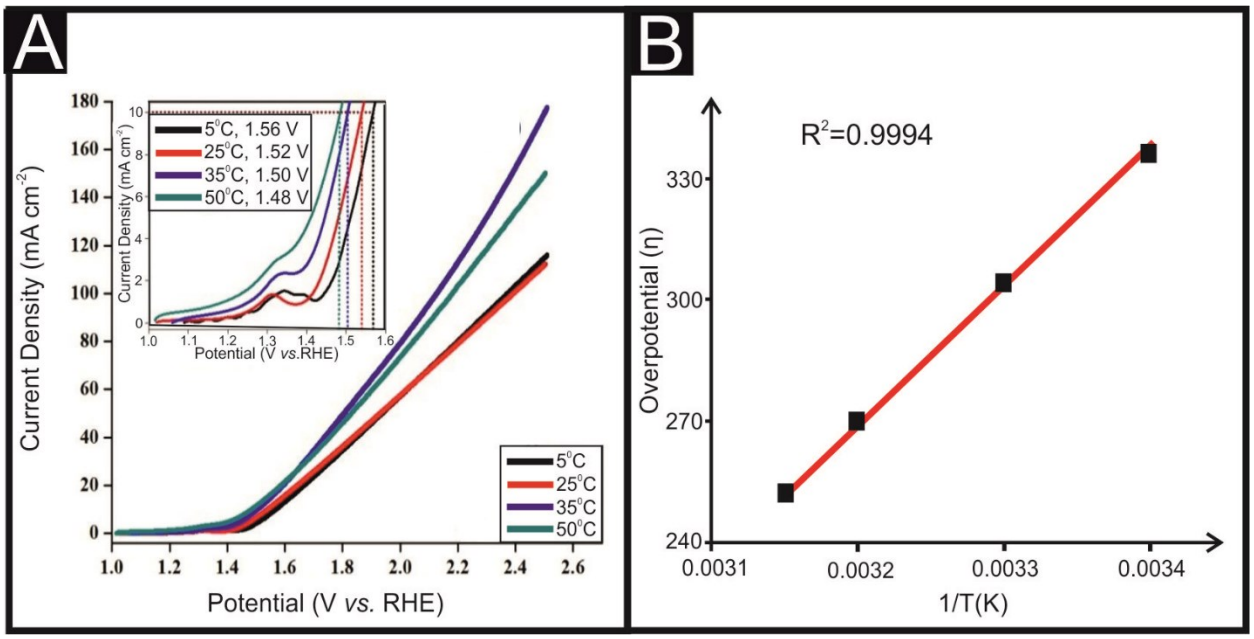

Table 1. Electrochemical active surface area calculated using Cdl values

Electrocatalysts	**Graphitic Co_3O_4**	**Nano Co_3O_4**	**Bulk Co_3O_4**	**Graphene oxide**
Electrochemical double layer capacitance ($mFcm^{-2}$)	35.70	31.56	19.18	17.58
Electrochemical active surface area (cm^2)	892.5	789	479.5	439.5